

This is an Open Access document downloaded from ORCA, Cardiff University's institutional repository:<https://orca.cardiff.ac.uk/id/eprint/102383/>

This is the author's version of a work that was submitted to / accepted for publication.

Citation for final published version:

Liu, Simeng, Pearson, Matthew R. , Eaton, Mark and Pullin, Rhys 2017. Correlation between acoustic emission distribution and stress variation through the depth of RC beam cross sections. *Construction and Building Materials* 150 , pp. 634-645. 10.1016/j.conbuildmat.2017.06.001

Publishers page: <http://dx.doi.org/10.1016/j.conbuildmat.2017.06.001>...

Please note:

Changes made as a result of publishing processes such as copy-editing, formatting and page numbers may not be reflected in this version. For the definitive version of this publication, please refer to the published source. You are advised to consult the publisher's version if you wish to cite this paper.

This version is being made available in accordance with publisher policies. See <http://orca.cf.ac.uk/policies.html> for usage policies. Copyright and moral rights for publications made available in ORCA are retained by the copyright holders.



1 Correlation between acoustic emission distribution and stress 2 variation through the depth of RC beam cross sections

3
4 LIU Simeng^{1,2}, Matthew R. Pearson³, Mark Eaton³, Rhys Pullin³

5
6 *1. State Key Laboratory Breeding Base of Mountain Bridge and Tunnel Engineering (Chongqing*
7 *Jiaotong University), Chongqing, P.R.China*

8 *2. School of Civil Engineering, Chongqing Jiaotong University, Chongqing, P.R.China*

9 *3. Cardiff School of Engineering, Cardiff University, Cardiff, Wales, UK*

10 11 **Highlights**

- 12 ● The acoustic emission distribution through the depth of RC beam sections is
13 studied.
- 14 ● AE parameters can characterise behaviours of RC beams in the depth direction.
- 15 ● AE event intensity shows a higher correlation than energy-based parameters in the
16 study.
- 17 ● The correlation between AE and stress responses was demonstrated to be very
18 strong.
- 19 ● A new option for estimating stress levels in engineering and science is considered.

20 21 **Abstract**

22 Two established techniques for monitoring concrete under loading are Acoustic
23 Emission (AE) and strain gauges. The distribution of strain, along with that of stress, on
24 a beam cross section is well established both theoretically and experimentally.
25 However, the AE distribution through the depth of the cross section has received little
26 attention previously. In addition, the correlation between the AE distribution and that
27 of stress on the section could provide valuable insight into the condition of a structure.
28 Therefore, these topics are experimentally addressed in this article. Specifically, six
29 Reinforced Concrete (RC) beams were tested. AE and Digital Image Correlation (DIC)
30 were employed to monitor the beams during loading. Finally, the AE and stress
31 distributions were analysed. The results showed that AE parameters are capable of
32 characterising behaviours of RC beams in the depth direction. Furthermore, the
33 distribution of AE events strongly correlated with that of compressive stress, especially

34 in the post-reinforcement yielding stage. According to these findings, it is highly
35 possible to estimate stress levels of RC beam structures in engineering and science by
36 adopting the AE technique.

37

38 **Keywords**

39 Acoustic Emission, Reinforced Concrete, compressive stress distribution, event intensity,
40 absolute energy, signal strength.

41 **1 Introduction**

42 Reinforced Concrete (RC) is one of the most extensively used materials in infrastructure,
43 including bridges, dams, tunnels and buildings. These structures are exposed to
44 deterioration or damage in service due to overloading, ageing, corrosion, fatigue, and
45 environmental hazards, etc. Acoustic Emission (AE) is a non-invasive and passive
46 Non-Destructive Testing (NDT) approach. AE may be defined as the transient elastic
47 waves that are generated by the rapid release of energy from damage sources within a
48 material [1]. AE techniques have been applied to damage diagnosis in civil engineering
49 for decades, for example, on RC structures [2-7], pre-stressed concrete (PC) structures
50 [8-11], glass fibre reinforced composite bridge decks [12] and constructions
51 strengthened with carbon fibre reinforced polymer (CFRP) [13-17]. Compared with
52 other methods, AE techniques have distinctive features. For instance, developing cracks
53 can be located [18].

54 AE-related concrete research has been carried out for decades, and includes

55 concrete crack classification, damage assessment and non-destructive monitoring. Hu, et
56 al. [5], investigated concrete crack propagation using AE techniques to determine the
57 initial load, crack propagation and final concrete structure failure. Rouchier, et al. [19],
58 used two parameters, the number and amplitude distribution of AE signals, to assess
59 cracking damage. Mohamed, et al. [20], studied the use of AE acquired during loading
60 as a substitute for conventional deformation measurements to assess the integrity of PC
61 beams. Ohtsu and Mori, et al. [21], compared the total number of AE hits with a
62 phenomenological model of steel embedded in concrete subjected to marine
63 environments, and showed that the two curves are in a remarkable agreement. Jochen
64 [22] presented a new concept of automatic AE three-dimensional source localization
65 based on developments from geodesy and ideas from seismology. Vishnuvardhan, et al
66 [23], characterised the sensitivity of active-sensing acousto-ultrasound-based Structural
67 Health Monitoring (SHM) techniques with respect to damage detection, and identified
68 the parameters that influence their sensitivity. The studies discussed above have shown
69 that AE parameters can be related to damage variables/indices, different failure
70 mechanisms and corrosion loss for steel in RC beams.

71 More work specifically linked to this investigation. Vidya, et al. [24] focused on
72 evaluating stress levels according to AE measurements. The researchers conducted an

73 experimental study on the Kaiser effect at different stress levels on RC beams. Fu, et al.
74 [25], investigated if the Kaiser effect exists in both the Brazilian and bending tests, and
75 found that the cumulative AE events vs. stress curves are more suitable for AE
76 investigations than the cumulative AE energy vs. stress curve. Lehtonen, et al. [26],
77 explored the variety of geological and mechanical factors involved in in-situ rock stress
78 estimations, and concluded that stress measurement via the Kaiser Effect-based methods
79 is only likely to be successful if it is supported by key geological and other stress
80 measurement information. Tuncay and Obara [27] compared stress values obtained from
81 AE and the compact conical-ended borehole overcoming techniques, and found that in
82 some stages, the stress values obtained in AE tests were two or three times greater than
83 those obtained by the latter. In conclusion, many practitioners have linked common AE
84 parameters to stress via the Kaiser effect.

85 According to the literature reviewed in this paper, it is evident that the distribution
86 of AE through a cross section of a structure has so far received little attention; hence, we
87 carried out this investigation. This study also carefully examined the possible
88 correlation between the AE distribution and the stress distribution through the depth of
89 an RC beam.

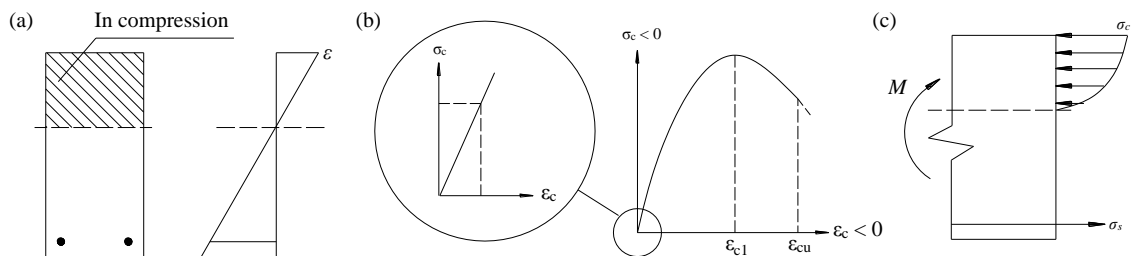
90

91 **2 Fundamental aims**

92 The Mechanics of Materials shows that strain develops linearly through the cross
93 sections of a structure under loading (e.g. Figure 1(a)). In addition, according to the
94 stress-strain relation of concrete (Figure 1(b)), different strain values correspond to
95 different stress magnitudes (Figure 1(c)), meaning that the pattern of the stress
96 distribution on the sections is deterministic and changes with load magnitudes. If the
97 magnitude of the load is sufficient, cracking occurs. Finally, well established research
98 [21, 28-33] has revealed that events, such as cracking, cause the release of energy in
99 materials, forming elastic waves, i.e. AE. Therefore, the following two questions are
100 considerably interesting in science and engineering:

- 101 1) How does the AE response vary through the cross sections?
102 2) What relations between AE and stress may exist during loading on the RC beam
103 structure to failure?

104



105

106 **Figure 1.** (a) A typical theoretical distribution of strain on an RC beam cross section; (b)

107 a stress-strain curve of the concrete material [34]; (c) the corresponding stress diagram
108 across the section.

109

110 Accordingly, in this study, six RC beams were tested, and the relationship between

111 stress/strain levels and AE signal properties were investigated. The primary attention

112 was paid to the possible correlations between structural and AE response distributions

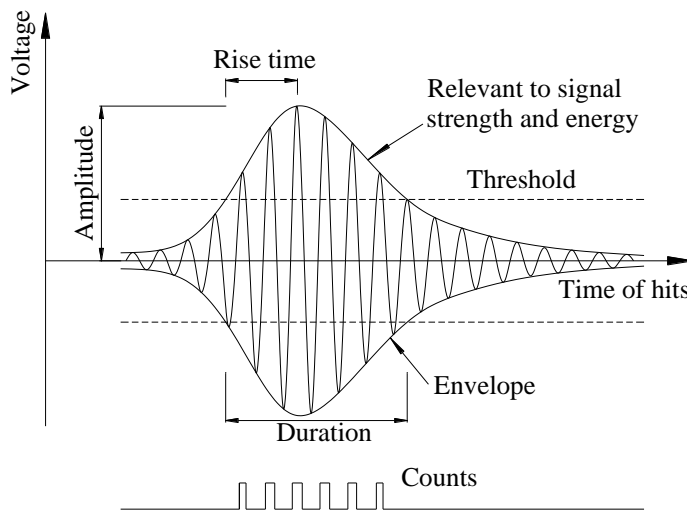
113 through a RC beam cross section. Figure 2 presents the classic AE parameters used to

114 describe waveforms and perform characterisation of signals [24]. Meanwhile, a new

115 term, called the AE event intensity, was introduced and was referred to the number of

116 AE events acquired per unit area.

117



118

119 **Figure 2.** Important AE-related concepts discussed in this paper.

120

121 **3 Experiment setup**

122 **3.1 Experimental specimens**

123 Six RC beam specimens were tested in this study. The beams were cut from a previous
124 experiment. All specimens were carefully examined before being tested in this study to
125 make sure that no severe damage had occurred.

126 The details of these specimens are shown in Figure 3 and Table 1. The sections of
127 all beams are rectangular, 120mm wide and 150mm or 155mm deep, with a clear span
128 of 620 mm (Table 1). In every specimen, one steel bar (N1), 12 mm in diameter, is
129 provided as tensile reinforcement, and another bar (N2), 6 mm in diameter, is used as
130 compressive reinforcement. Stirrups (N3), 6 mm in diameter, are placed at 50 mm c/c
131 distance to avoid shear failure. The beams were designed in accordance with British
132 Standard for grade C40, and the mixture proportion of the concrete was that cement :
133 fine aggregate : coarse aggregate : water = 1:2:3:0.5, by weight. Steel fibres, 30mm or
134 60mm long, were mixed in the concrete, with a ratio of 1% or 2% (by weight), to obtain
135 the Steel Fibre Concrete (SFC). The specimens were cast in a specially made wooden
136 mould and a standard steel mould, and compacted using a needle vibrator.

137

138 **Table 1.** The dimensions, materials and test results of all six RC specimens

No.	Sectional sizes/mm Height x Width	Material	Strength/kN	Failure mode
-----	--------------------------------------	----------	-------------	--------------

Beam 1	155x120	SFC ,2%, 30mm	83.41	Bending failure
Beam 2	150x120	Concrete, C40	68.12	Shear failure
Beam 3	150x120	Concrete, C40	68.05	Bending failure
Beam 4	155x120	SFC ,1%, 60mm	85.20	Bending failure
Beam 5	155x120	SFC ,1%, 60mm	79.62	Bending failure
Beam 6	155x120	SFC ,2%, 30mm	82.43	Bending failure

139

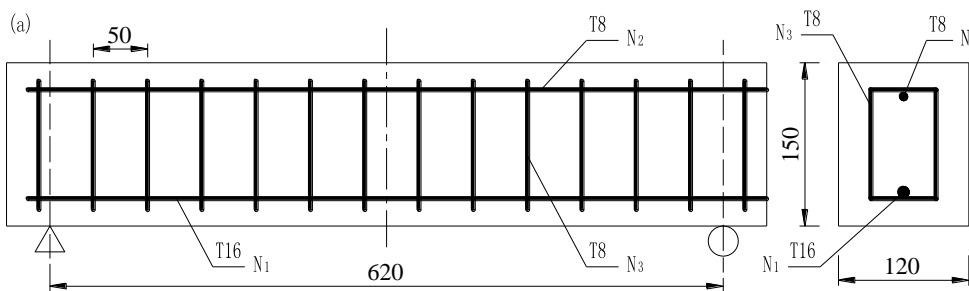
140 To promote the failure of every beam at its mid-span, a 10 mm deep notch was

141 made. After they were tested, Beams 5 and 6 were cut in half at the failed positions, and

142 the depths of crushed concrete and the lengths of major cracks were then measured.

143

144



145

146 **Figure 3.** (a) The design details of the simply supported RC beams tested in the study

147 (Units in mm), (b) a photo of all specimens.

148

149 **3.2 Instrumentation**

150 AE signals were recorded with a MISTRAS system. The system consisted of
151 preamplifiers (40dB), R6D sensors (40–100 kHz) and a personal computer (PC) with
152 eight AE channels. A full suite of the AEWIn software was installed on the PC. The
153 acquisition parameters adopted in the study are listed in Table 2.

154

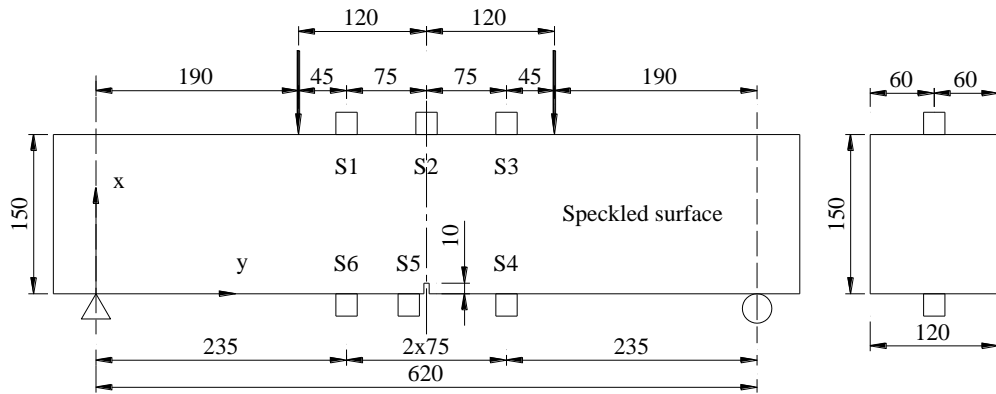
155 **Table 2.** The parameters used during AE data acquisition.

Parameter	Value
Threshold	45 dB
Velocity	4030 m/s
Hit definition time (HDT)	800 ms
Peak definition time (PDT)	200 ms
Hit lockout time (HLT)	1000 ms

156

157 As stated by Swit [35], since AE signals are mainly registered by sensors that are
158 close enough to the sources of AE events, all sensors were therefore placed around the
159 most probable site of damage – the notch and the pure bending region. Hence, as shown
160 in Figure 4, six sensors (S1 through S6) are mounted on the top and the bottom of every
161 beam. Brown grease was used as an acoustic couplant. Sensor S5 is placed adjacent to
162 each pre-cut notch. In order to make sure all sensors were mounted correctly, a
163 Pencil-Lead Breaks (PLBs) [36] test was completed prior to testing.

164



S1 ~ S6 : Acoustic Emission Sensor 1 to 6.

165

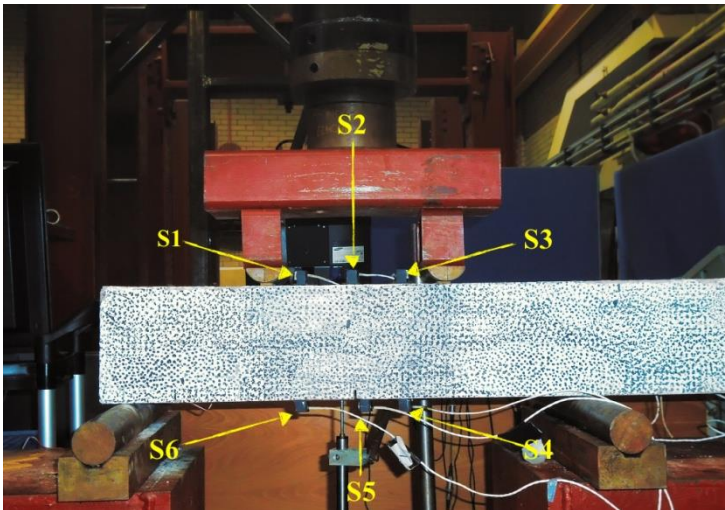


Figure 4. The layout of all six AE sensors employed in tests (Units in mm).

166

167

168

169

Other instruments used in the study included a digital image correlation (DIC)

170

system, strain gauges and displacement transducers. In order to estimate the strain

171

distribution on a side surface of each RC beam, DIC was employed. The area of interest

172

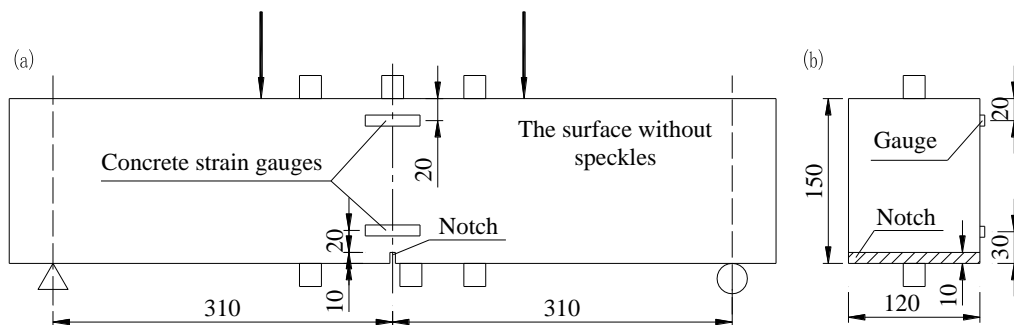
on Specimen 1 was the whole side surface, while on the others the DIC cameras just

173

focused on the region under pure bending (Figures 4 and 5). Meanwhile, two electric

174 resistance wire concrete strain gauges were affixed to measure point strain. As shown in
 175 Figure 5, one gauge is 20mm away from the top of the beam, and the other is 20mm
 176 away from the top of the notch. In addition, a displacement transducer was arranged
 177 beneath the mid-span of each specimen.

178



179

180 **Figure 5.** The layout of two concrete strain gauges on each beam: (a) Elevation, (b) The
 181 mid-span cross-section diagram (Units in mm).

182

183 **3.3 Loading conditions**

184 As shown in both Figures 4 and 5, each specimen is subjected to four-point bending.

185 The loads increased monotonically with a rate of 0.005mm/s until one of the following

186 two criteria was satisfied. The first was that a part of the specimen was crushed

187 completely, which led to the failure of the structure, and the other was the loads dropped

188 from peak by 20% or greater.

189

190 **4 Results**

191 In this Section, data obtained on Beam 1 are discussed extensively to examine the AE
192 activity across the depth of the beam. Meanwhile, some data of the other specimens are
193 also presented herein for the purpose of cross checks. Furthermore, several details are
194 explained as follows prior to further data analysis.

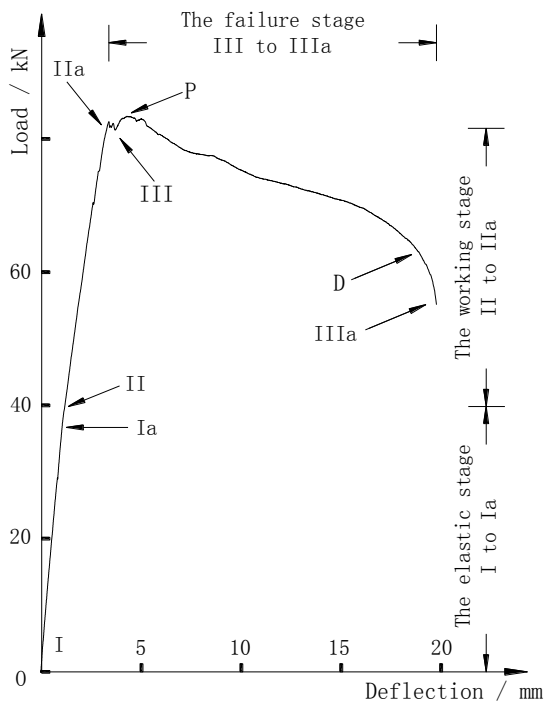
195 Data acquired just in a specific region on each specimen and in some stages during
196 testing are discussed in the following parts. More specifically, the volume surrounded
197 by all six AE sensors are treated as one “single” section, and just AE signals from it are
198 analysed. Namely, AE events whose x- and y-coordinates satisfy $235\text{mm} \leq x \leq 385\text{mm}$
199 and $0 \leq y \leq 155\text{mm}$ (for Beams 1, 4, 5 and 6) or $0 \leq y \leq 150\text{mm}$ (only for Beams 2 and 3)
200 are considered hereafter, referring to Figure 4 for the coordinate definition. The reasons
201 are as follows. Firstly, in practice, it is impossible to acquire AE signals from a real
202 cross section. Secondly, the volume, with a length equal to only the beam depth (Figure
203 4), is very short, and all cross sections in the volume are subjected to bending moment
204 of the same magnitude. Simultaneously, the following analyses focus on processing AE
205 signals recorded during some typical stages and states of every RC beam. The reason
206 lies in that they indicate significant changes in cracks and decrements in stiffness or
207 load bearing capacity of the structure.

208 Three AE descriptors, namely AE event intensity, absolute energy and signal
209 strength, were used in this study. In addition, strain and stress levels of specimens are
210 estimated based on the measurements provided by the two concrete strain gauges and
211 the DIC system. Furthermore, strain diagrams are calculated using the curve-fitting
212 approach and stress diagrams are obtained by combining the stress-strain relation of the
213 concrete material[32] with the strain estimations.

214 ***4.1 Typical loading stages and structural states of RC beams***

215 The failure of Beam 1, i.e. a three-stage loading process, is detailed as follows. In the
216 first stage, no cracks were observed, and the stiffness of the beam was of the greatest
217 magnitude. Theoretically, all parts of each cross section are effective in resisting
218 external moment, and concrete stress is proportional to strain. The stage corresponds to
219 *I-Ia* in the first panel of Figure 6. In the second stage, cracks appeared in the tensile
220 zone very close to the notch, and the deflection of the beam increased significantly,
221 meaning its stiffness also appreciably declined. In theory, the stress increases with strain
222 nonlinearly, and to a cracked section, only a part of the section provides resistance to the
223 bending moment. The second stage corresponds to *II-IIa* in Figure 6. In the third stage,
224 many cracks appeared in both the tensile and compressive regions; and strain increased
225 rapidly until the bearing capacity of the beam was reached; simultaneously, tensile

226 reinforcement yielded. More importantly, the stiffness dramatically reduced. Finally, a
227 part of the concrete in the compressive region was crushed, and then the beam
228 completely failed (See the lower panel of the figure). The last stage corresponds to
229 *III-IIIa* in Figure 6.
230



231



232
 233 **Figure 6** The load-deflection curve (Upper) and the failure shape (Lower) of Beam 1.
 234

235 The above description regarding the failure of Beam 1 is in line with established
 236 research [34, 37-39]. Testing of RC beam structures can be divided into several
 237 important stages, and these stages can be identified on a load vs. deflection curve, such
 238 as the upper panel of Figure 6. Accordingly, all critical stages studied in subsequent
 239 parts are listed in Table 3. More importantly, their significance in structural respects is
 240 also introduced briefly. Additionally, several critical states listed in Table 3 and Figure 6
 241 are also investigated later.

242
 243 **Table 3.** Critical stages and states of a typical RC beam loaded to failure.

Stages / states	Structural significance	Notations
The elastic stage	No crack develops, and the beam behaves elastically.	<i>I to Ia</i>
The working stage	Cracks develop in tensile regions, and the stiffness therefore decreases slightly.	<i>II to IIa</i>
The failure stage	Cracks also appear in compressive regions. Reinforcement yields. The bearing capacity and	<i>III to IIIa</i>

	stiffness decline significantly.	
Yielding of reinforcement	The reinforcement in tension yields	<i>Ia to II</i>
Peak load	The beam reaches its ultimate bearing capacity.	<i>III to P</i>
Load decline	The bearing capacity decreases rapidly.	<i>P to D</i>

244

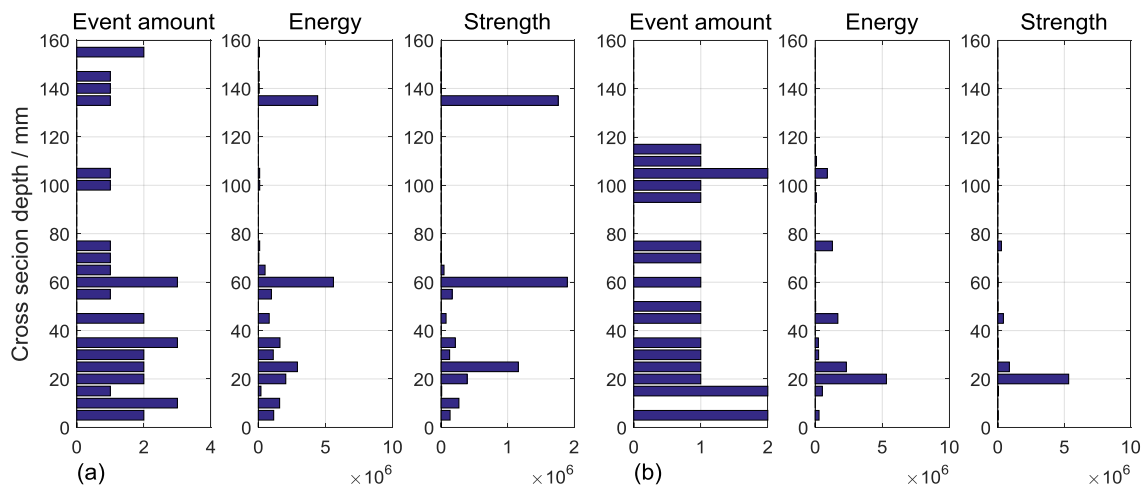
245 When results are presented as follows, two approaches are employed. The first is to
 246 show the AE response in a specific stage. The second is to assess data acquired from the
 247 start of the test until the end of the current loading stage, namely the accumulated data.

248

249 ***4.2 In the elastic stage of RC beams***

250 Figure 7 shows the AE data of Beam 1 obtained in the elastic stage and during the
 251 period from *Ia* to *II*. Note that the y-axis of all figures is the depth of RC beam section.
 252 The cross-sectional height (155mm) is divided into 31 intervals, and three variables, i.e.
 253 the AE events, absolute energy and signal strength, are related to each interval (5mm
 254 high). When an event is located in an interval, the AE event amount variable increases
 255 by one, and the quantities of the energy and the signal strength are added to the other
 256 two variables, respectively. The x-coordinate is the amount of AE events (proportion to
 257 the intensity), absolute energy or signal strength. Note that the total number of events
 258 identified is 3,649, and the order of magnitude of the AE absolute energy and the signal
 259 strength in the failure state of Beam 1 is 10^8 .

260



261

262 **Figure 7** The distributions of the acoustic emissions acquired (a) in the elastic stage and
263 (b) during the onset of the first crack in the tensile area, across the depth of Beam 1
264 (Energy refers to the AE Absolute Energy, in aJ (attojoules); Strength is short for the
265 Signal Strength, in pVs (picovolt-seconds)).

266

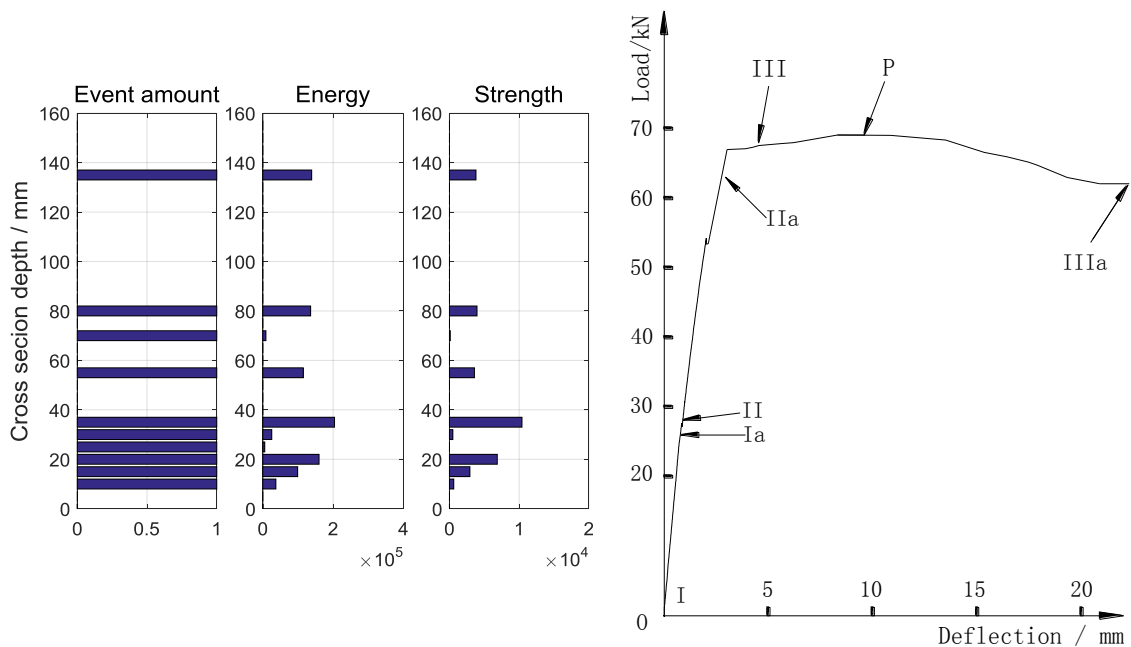
267 As shown in the left panel of Figure 7, there are 31 AE events acquired within the
268 elastic stage of loading. The number is less than 1% of the total event amount (3,649),
269 demonstrating AE activity is very low. Furthermore, structural responses of the beam
270 can give deep insight into the characteristic of showing low AE activity at this stage.
271 Since the maximum tensile stress in the concrete is smaller than the modulus of rupture
272 at this stage, all parts of a concrete section are effective in resisting stress which is
273 proportional to strain[34, 37-39]. Namely, the beam is behaving elastically.
274 Theoretically, it is therefore, generally assumed that no damage has occurred [40].
275 Consequently, the AE activity inside the beam is very low. In conclusion, the structural

276 responses come to a very good agreement with the AE detected.

277 The first crack appeared during the period from *Ia* to *II* in Figure 6, and Figure 7
278 shows the corresponding AE measurements. The second panel of Figure 7 reveals that
279 19 AE events were recorded, similar to what happened in the previous stage. Therefore,
280 the AE activity in this period is also considered to be considerably low. However, as
281 shown in the load vs. deflection curve (Figure 6), the slope of the curve in the
282 post-elastic stage decreases slightly, meaning that the stiffness has reduced. For
283 comparison, the data from the same stage of testing in Beam 3 is shown in Figure 8 and
284 support the the above conclusions.

285

286



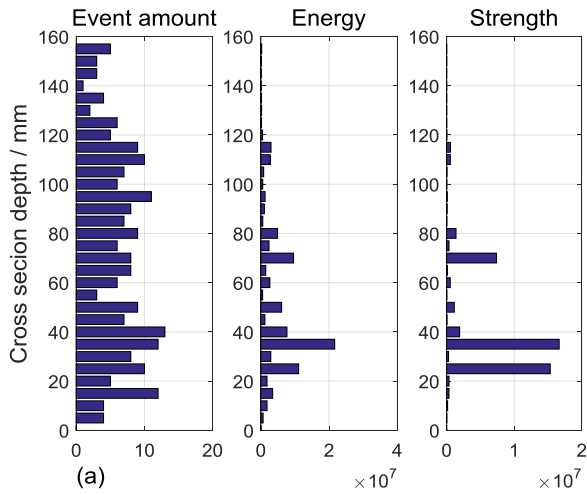
287 **Figure 8** The distributions of the acoustic emissions acquired in the elastic stage
288 through the depth (Left) and the load-deflection curve (Right) of Beam 3

289

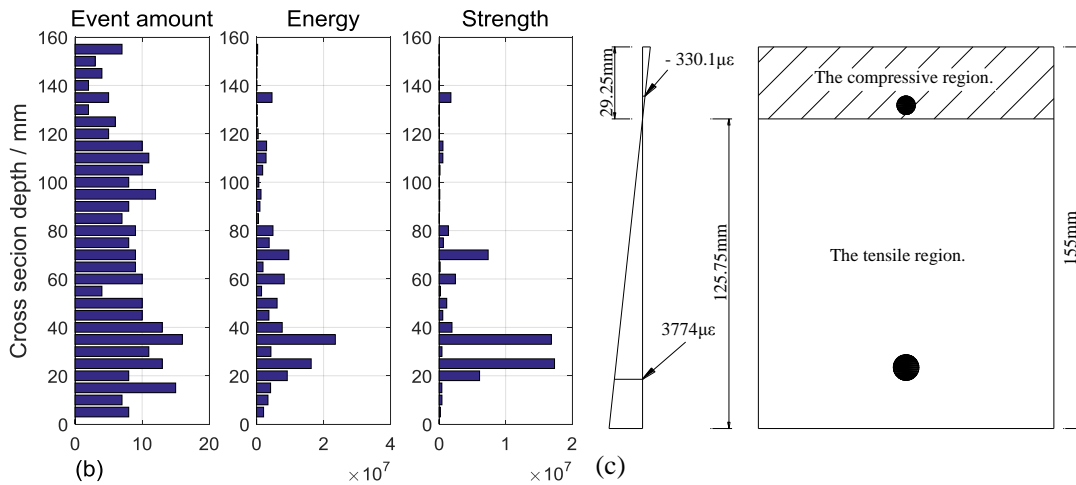
290 ***4.3 In the working stage of RC beams***

291 As shown in Figure 9, two features are considerably obvious at this stage. Firstly, 211
292 events, 581% larger than the amount of emissions captured in the elastic stage, were
293 acquired on Beam 1, meaning that the AE activity significantly increased. However, the
294 activity is still low as it represents only 5.78% of the total number of the events captured
295 in the entire test. Secondly, most of the events took place in the tensile zone of the beam,
296 meaning the AE event distribution roughly matched with that of the tensile stress (the
297 right panel in Figure 9). Meanwhile, the intensity of AE events in the compressive
298 region also rose. In addition, analysing the data of the AE absolute energy came to
299 similar conclusions, and the same characteristics were also found on the other
300 specimens, which are not presented here to save space.

301



302



303

304 **Figure 9** The distributions of the acoustic emissions acquired (a) in the working stage,
 305 (b) until the end of the stage and (c) the corresponding total strain distribution through
 306 the depth of Beam 1.

307

308 **4.4 In the failure state of RC beams**

309 For Beam 1, more than 90% AE events were captured in the failure stage; therefore, it is

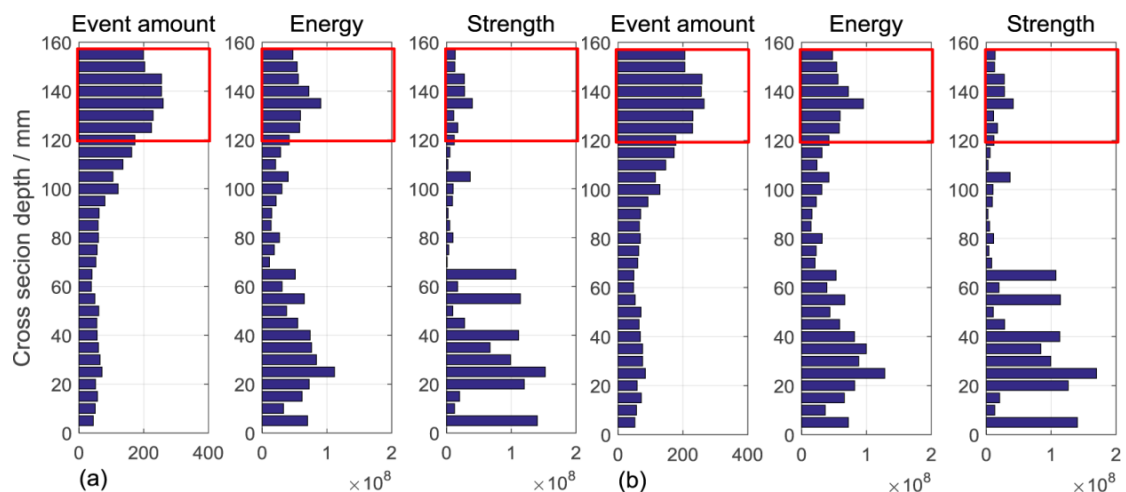
310 quite clear that the beam was very active in terms of AE. Meanwhile, several crucial

311 events, e.g. the yielding of reinforcement and the reaching of peak loads, occurred

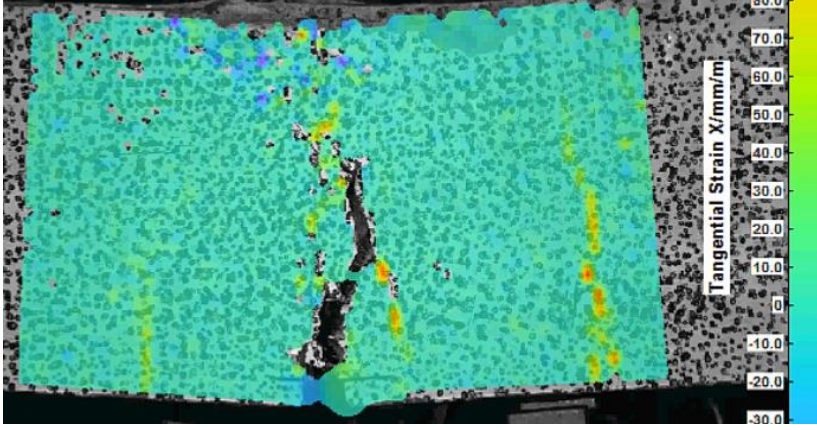
312 during this stage. Hence, the stage is analysed carefully as follows.

313 In Figure 10, all AE and DIC data acquired in the failure stage (Panel (a)) and
314 throughout the test (Panels (b) and (c)) are presented, while further analysis on the
315 corresponding behaviour of Beam 1 is shown in Figure 11. On the whole, Figure 10
316 shows two features. Firstly, the AE activity dramatically rises in the stage. For example,
317 as shown in Panels (a) and (b), the order of magnitude of the AE absolute energy and
318 signal strength is 10^8 , while it is 10^7 in the previous stage. Secondly, the AE event
319 intensity in the compressive zone is far greater than that in the tensile region. Both
320 features are also observed on other specimens, such as Beam 4 (Figure 12). Additionally,
321 other researchers [19] also came to the same conclusion, namely overwhelming majority
322 of AE events appear during the final failure of structures.

323



324



325

326 **Figure 10** The distributions of the acoustic emissions acquired (a) in the failure stage,
 327 (b) until the end of the test and (c) the corresponding total strain distribution through
 328 the depth of Beam 1(The compressive concrete zone is circled with red rectangles).
 329

329

330 More importantly, an insight into the AE results comes from the examination of the
 331 correlation between the AE event intensity distribution and that of the stress in the
 332 compressive zone (Figure 11). To analyse the correlation, the following three steps are
 333 needed. Firstly, in Panel (a), the strain over the mid-span section of Beam 1 is calculated
 334 according to the data (Figure 10(c)) obtained with the DIC device in the ultimate state.
 335 Secondly, in Panel (b), the stress in the compressive zone is calculated according to the
 336 stress-strain relation (Eq. (1)) [34].

338
$$\frac{\sigma_c}{f_{cm}} = \frac{k\eta - \eta^2}{1 + (k - 2)\eta}$$

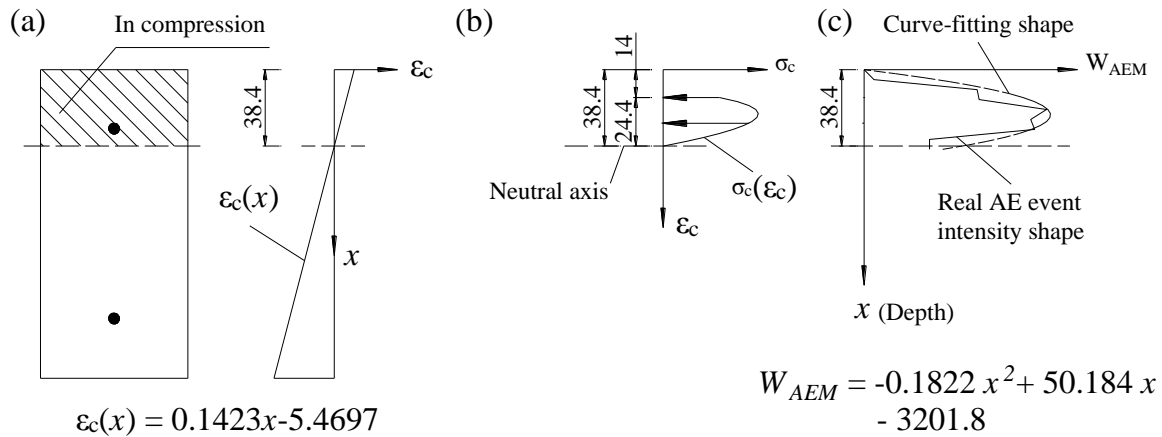
337 (1)

339
$$\eta = \frac{\varepsilon_c}{\varepsilon_{c1}}, \quad \varepsilon_c \leq 0.0035, \quad k = \frac{1.05E_{cm} \times |\varepsilon_{c1}|}{f_{cm}}$$

340

341 where σ_c is the compressive stress value when strain is $\varepsilon_c(\leq 0.0035)$, and ε_{c1} is the
342 strain at peak stress. f_{cm} and E_{cm} are the mean compressive strength at 28 days and
343 the modulus of elasticity, respectively. ε_{c1} , f_{cm} and E_{cm} are specified in the code[34].
344 Note that only the compressive stress is considered here, because the concrete in the
345 tensile zone has been cracked due to vulnerability of the material [41]. Finally, the
346 distribution of the AE through the depth of the compressive zone is estimated using the
347 curve-fitting approach (Panel (c)). Note that in Panel (b), there is a blank (14mm high)
348 on the top of the section. This attributes to the excessive strain over the region. Eq. (1) is
349 just applied to cases where $\varepsilon_c \leq 0.0035$ (Figure 1(b)), however, ε_c in the blank
350 region does not satisfy the condition. Hence, the stress over the region cannot be
351 computed according to Eq.(1). In fact, $\varepsilon_c > 0.0035$ means that, physically, concrete
352 has been crushed. Additionally, the blank is confirmed in Figure 15 and is discussed in
353 Section 6 again.

354

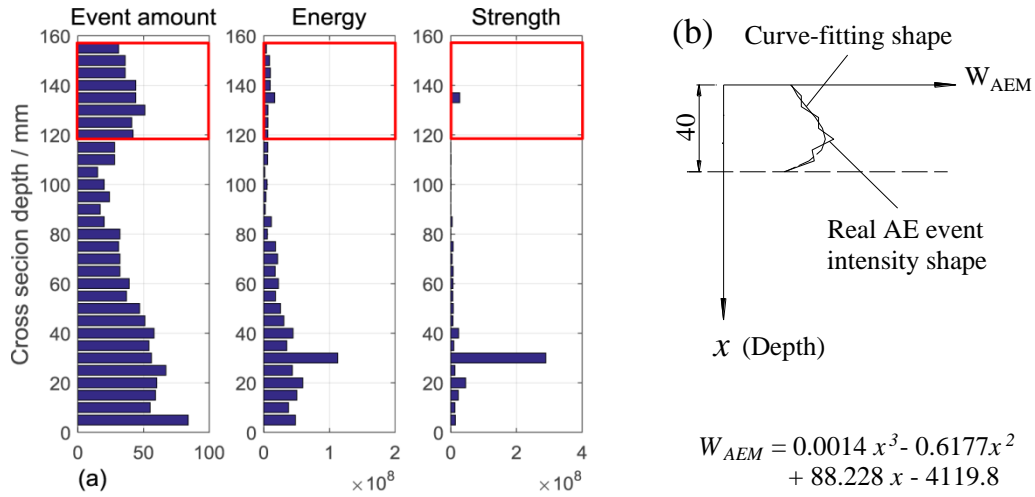


355
356
357
358
359

Figure 11 (a) The strain diagram on the mid-span section, (b) the corresponding stress distribution and (c) the AE event intensity distribution in the compressive region of Beam 1 (Length in mm, stress and strength in MPa).

360
361
362
363
364
365
366
367
368

As shown in Panels (b) and (c) of Figure 11, the distribution of the AE event intensity correlates very well with that of the compressive stress over the zone. Firstly, these two distributions are of very similar curve shapes. Secondly, the peak values of the AE event intensity and the stress occur at almost the same location. More specifically, the former appears 20mm away from the top, the latter 22mm. This was consistent in all beams and demonstrated by Figure 12 from Beam 4. In conclusion, the AE intensity variation pattern accurately correlates with the distribution of the compressive stress through the cross-sectional depth in the failure stage.



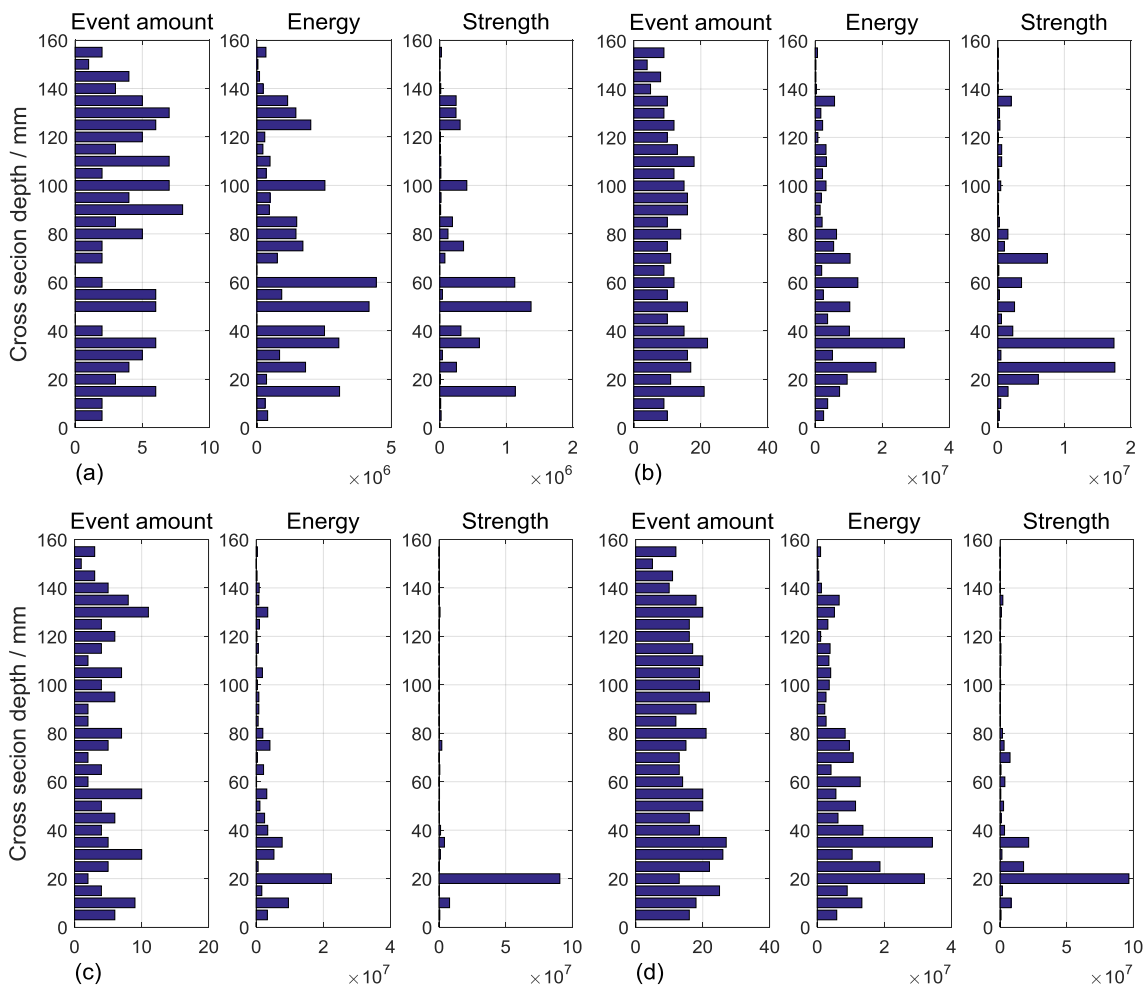
369

370 **Figure 12** (a) The distribution of the acoustic emissions acquired in the test on Beam 4
 371 through the depth and (b) the AE event intensity distribution over the compressive
 372 region circled with red rectangles (Length in mm).

373

374 Three critical issues, i.e. the yielding of reinforced steel bars, the peak loads and
 375 the decrease of the load, occurred during the failure stage, and they deserve further
 376 investigation. The AE data corresponding to the first two sub stages are illustrated in
 377 Figure 13. The figure shows that, compared with the AE response in the working stage,
 378 the AE activity does not increase significantly. More specifically, the AE event intensity
 379 remains at the same level, and the order of magnitude of the absolute energy and signal
 380 strength remains unchanged. However, the activity in the compressive zone begins to
 381 rise although it is still lower than that in the tensile region. In conclusion, the significant
 382 changes in AE activity shown in Figure 10 do not occur in these two periods of time.

383



384

385

386 **Figure 13** The distributions of the acoustic emissions acquired (a) during the yielding of
 387 reinforcement, (b) until the yielding of reinforcement, (c) during the period from III to
 388 P and (d) until the peak load, namely Point P, through the depth of Beam 1.

389

390

In fact, as shown in Figure 14, the beam experiences a dramatic increase in the AE

391

response when the loads drop from peak and the beam reaches ultimate failure. 82.85%

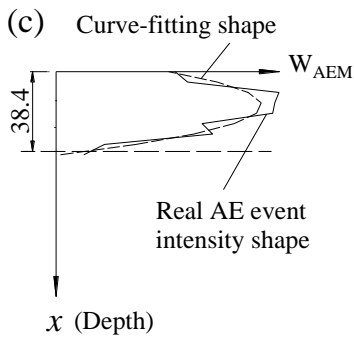
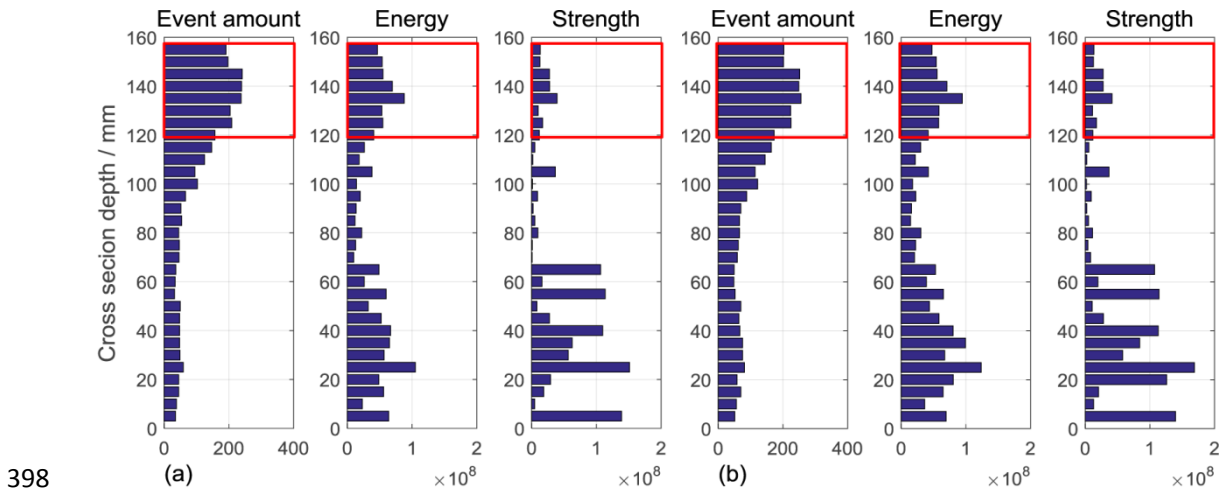
392

of all AE events occur in the duration. Furthermore, as showed in Panel (c), the shape of

393

the AE event intensity distribution curve closely matches the stress diagram (Figure

394 11(b)). Meanwhile, compared with the situations in the previous stages, the order of
 395 magnitude of the AE absolute energy and the signal strength rises from 10^7 to 10^8 .
 396 Accordingly, these data mean that Beam 1 shows the highest AE activity in this period.
 397



$$W_{AEM} = -0.171 x^2 + 47.474 x - 3062.3$$

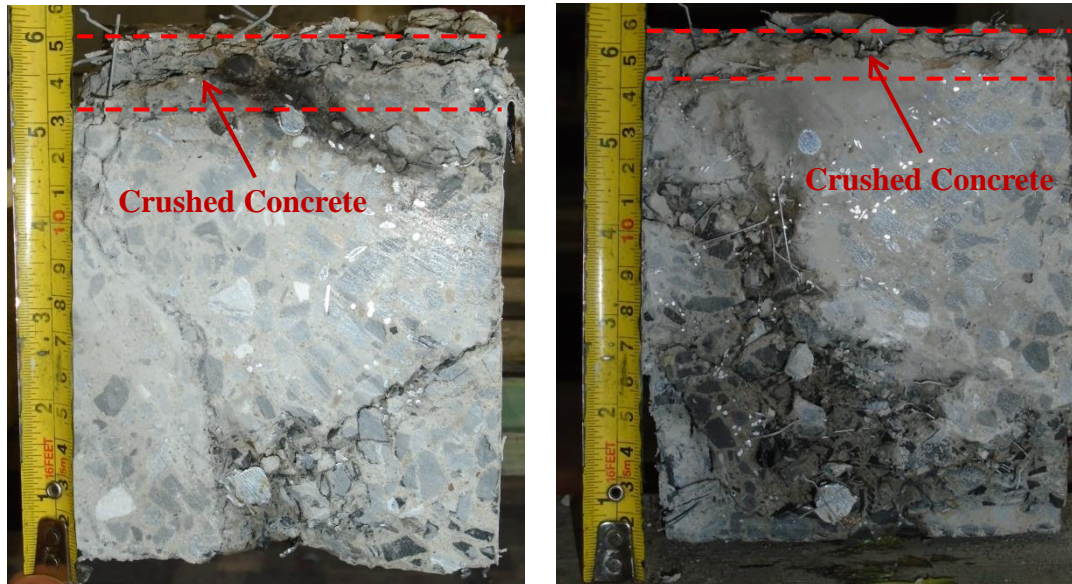
399
 400 **Figure 14** The distributions of the acoustic emissions acquired (a) during the period
 401 from P to D, (b) until the Point D across the depth of Beam 1 and (c) the AE event
 402 intensity distribution over the compressive region circled with red rectangles (Length
 403 in mm).
 404

405 **5 Discussions**

406 ***5.1 Observations from cut cross sections***

407 Beams 5 and 6 were cut at the failed sections after final failure. As shown in Figure 15,
408 two conclusions can be drawn based on observations from the cut sections. Firstly, the
409 thickness of the crushed concrete measured in Figure 15 matches with the estimation
410 (14mm high) in Figure 11(b). In the discussion regarding the zero-stress zone in Figure
411 11(b), it was theoretically concluded that the concrete on the top of the section was
412 crushed, which resulted in the 14mm-depth interval with zero stress. It is confirmed
413 here, and the thickness of the crushed concrete measured in Figure 15, ranging from
414 13mm to 20mm (the space in between the two pairs of red dashed lines), matches very
415 well with the estimation (14mm). Secondly, AE events occurred through the whole
416 depth. This conclusion is supported by the observation that cracks developed during
417 testing had penetrated through almost the entire cross section. This is very strong
418 evidence of the AE distributions shown in Figures 9, 10, 12, and 13. In conclusion,
419 these observations strongly support the outputs discussed previously.

420



421

422 **Figure 15** The cut cross sections of Beams 5 (Left) and 6, respectively.

423

424 **5.2 AE on the specimen that failed in the shear mode**

425 Only Beam 2 failed in the shear mode (See Table 1 and Figure 16). The AE variation

426 across the depth of the beam is distinctively different from those that failed in the

427 flexural mode. Firstly, as shown in the left panel in Figure 16, the amount of AE events

428 acquired in the compressive region is far less than that from the tensile area. The lower

429 activity in the compressive region of Beam 2 means that the damage level is relatively

430 low, suggesting the stress level of the beam is also low. More importantly, this indicates

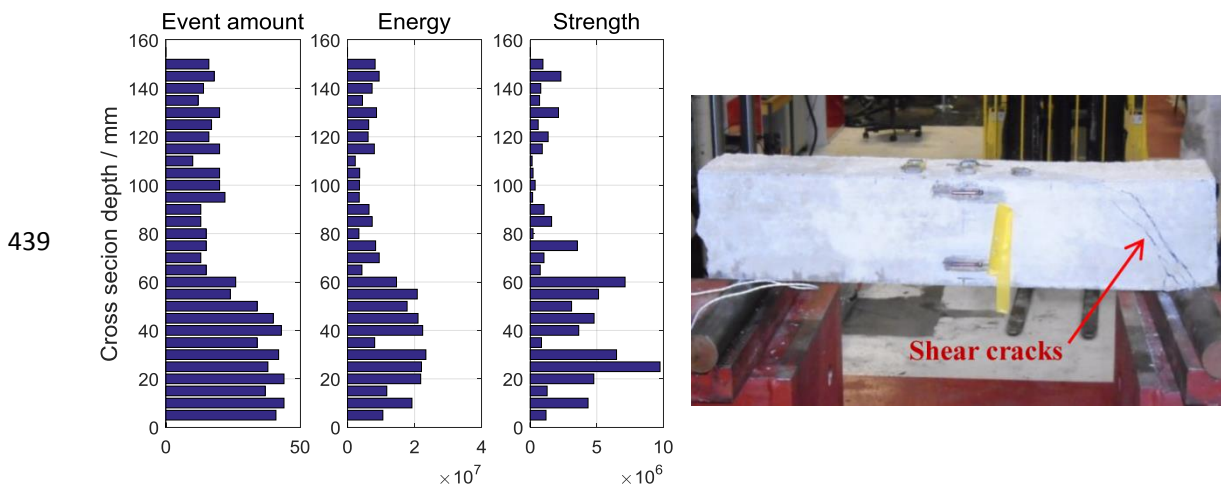
431 that the strength potential of the concrete is not fully used due to the occurrence of the

432 shear failure. Secondly, the AE absolute energy and the signal strength of Beam 2 are at

433 least one order of magnitude smaller than that of the other specimens. As shown in

434 Figures 10, 11 and 14, on Beam 2, the order of magnitude is 10^7 or 10^6 , while that of
 435 beams failed in the flexural mode is 10^8 . This also indicates the material in Beam 2 is
 436 not completely utilised, and the conclusion matches with findings in traditional concrete
 437 structure research [38, 39].

438



440 **Figure 16** The distribution of the AE acquired through the test on Beam 2 (Left) and the
 441 shape when it failed (Right).

442

443 6 Conclusions

444 This study focused on AE distribution through the depth of an RC beam and the
 445 correlation between AE and stress variations. Experiments on six beams were conducted,
 446 and all critical stages of these beams, i.e. the elastic stage, the working stage and the
 447 failure stage, were examined carefully. AE response, structural deflections and
 448 strain/stress were measured and then analysed in detail. Based on this work, the

449 following conclusions were drawn:

- 450 ● AE is highly capable of characterising the behaviours through the depth of RC
451 beams. Furthermore, the AE event intensity outperformed the absolute energy
452 and the signal strength in the study.
- 453 ● In the elastic stage, the AE activity was very low. For example, less than 1% of
454 the total amount of AE events were acquired on Beam 1, and the order of
455 magnitude of both the AE absolute energy and the signal strength was 10^6
456 (Figure 7).
- 457 ● In the working stage, the AE activity rose slightly, however, it was not yet very
458 high. More specifically, only about 5% of the total AE events were recorded.
459 The order of magnitude of the absolute energy/signal strength was 10^7 (Figure
460 9). Meanwhile, the AE response distribution matched with that of the stress
461 distribution.
- 462 ● In the failure stage, the overwhelming majority of AE were captured, meaning
463 that specimens were considerably active. More than 90% of the total AE events
464 were recorded, and the order of magnitude for energy was 10^8 (Figure 10).
465 Nevertheless, the beam was relatively inactive during yielding of reinforcement

466 and at peak load (Figure 13). However, the AE was highly active when the loads
467 dropped from peak (Figure 14).

468 ● The most significant finding in the study is that the distribution of the AE event
469 intensity accurately matches with that of the stress over the compressive zone.
470 (Figures 11, 12 and 14). Namely, the pattern of AE event intensity distribution
471 in the depth direction is very similar to the compressive stress diagram.
472 Meanwhile, the peak of the AE event intensity and the stress appears at almost
473 the same location.

474 The above conclusions suggest that the AE technology is of great potential to serve
475 as a measure to estimate critical stress levels of RC beam structures. This topic is
476 addressed in another article. Note that the idea, determining critical stress states in
477 structures via AE parameter distribution analysis, deserves researchers and practisers'
478 more work to extend it to more scenarios and inspire more innovations.

479 **Funding**

480 This work was funded by the Open Fund of State Key Laboratory Breeding Base of
481 Mountain Bridge and Tunnel Engineering (Chongqing Jiao tong University) and Key
482 Laboratory of Bridge Structure Engineering Transportation Industry (Chongqing)
483 (CQSLBF-Y15-2), National Natural Science Foundation of China (51508058,
484 51479013), Youth Science and Technology Talent Cultivating Plan of Chongqing City
485 (cstc2014kjrc-qnrc30001).

486 **Acknowledgement**

487 The authors highly appreciate the contributions from technicians, Carl Wadsworth, Ian
488 King, Jack Morgan and Richard Thomas; faculty members, John McCrory, Davide
489 Crivelli and Ryan Marks; Ph.D. candidates, ZAC (王宇) and Stephen Grigg in Cardiff
490 School of Engineering, Cardiff University, Wales, United Kingdom.

491 **References**

- 492 [1] N.M. Nor, A. Ibrahim, N.M. Bunnori, H.M. Saman, S.N.M. Saliyah, S. Shahidan, Diagnostic of fatigue
493 damage severity on reinforced concrete beam using acoustic emission technique, *Engineering Failure*
494 *Analysis* 41(5) (2014) 1-9.
- 495 [2] Z. Liu, P.H. Ziehl, Evaluation of Reinforced Concrete Beam Specimens with Acoustic Emission and
496 Cyclic Load Test Methods, *Aci Structural Journal* 106(3) (2009) 288-299.
- 497 [3] M.A.A. Aldahdooh, N.M. Bunnori, Crack classification in reinforced concrete beams with varying
498 thicknesses by mean of acoustic emission signal features, *Construction & Building Materials* 45(45) (2013)
499 282–288.
- 500 [4] M.A.A. Aldahdooh, N.M. Bunnori, M.A.M. Johari, Damage evaluation of reinforced concrete beams
501 with varying thickness using the acoustic emission technique, *Construction & Building Materials* 44(44)
502 (2013) 812-821.
- 503 [5] S. Hu, J. Lu, F. Xiao, Evaluation of concrete fracture procedure based on acoustic emission parameters,
504 *Construction & Building Materials* 47(47) (2013) 1249-1256.
- 505 [6] N.M. Nor, A. Ibrahim, N.M. Bunnori, H.M. Saman, Acoustic emission signal for fatigue crack
506 classification on reinforced concrete beam, *Construction & Building Materials* 49(6) (2013) 583-590.
- 507 [7] S. Shahidan, R. Pulin, N.M. Bunnori, K.M. Holford, Damage classification in reinforced concrete beam
508 by acoustic emission signal analysis, *Construction & Building Materials* 45(13) (2013) 78–86.
- 509 [8] P.H. Ziehl, Early corrosion monitoring of prestressed concrete piles using acoustic emission, *Spie*
510 *Smart Structures & Materials + Nondestructive Evaluation & Health Monitoring*, 2013, pp.
511 869407-869407-11.
- 512 [9] M. Abdelrahman, M.K. Elbatanouny, P.H. Ziehl, Acoustic emission based damage assessment method
513 for prestressed concrete structures: Modified index of damage, *Engineering Structures* 60(60) (2014)
514 258-264.
- 515 [10] W. Vélez, F. Matta, P. Ziehl, Acoustic emission monitoring of early corrosion in prestressed concrete
516 piles, *Structural Control & Health Monitoring* 22(1) (2014) 873–887.
- 517 [11] R. Anay, T.M. Cortez, D.V. Jáuregui, M.K. Elbatanouny, P. Ziehl, On-Site Acoustic Emission Monitoring
518 for Assessment of a Prestressed Concrete Double-Tee-Beam Bridge without Plans, *Journal of*

519 Performance of Constructed Facilities 04015062 (2015) 1-9.

520 [12] R.S. Gostautas, G. Ramirez, R.J. Peterman, D. Meggers, Acoustic Emission Monitoring and Analysis of
521 Glass Fiber-Reinforced Composites Bridge Decks, *Journal of Bridge Engineering* 10(6) (2005) 713-721.

522 [13] S. Degala, P. Rizzo, K. Ramanathan, K.A. Harries, Acoustic emission monitoring of CFRP reinforced
523 concrete slabs, *Construction & Building Materials* 23(5) (2009) 2016-2026.

524 [14] H.D. Yun, W.C. Choi, S.Y. Seo, Acoustic emission activities and damage evaluation of reinforced
525 concrete beams strengthened with CFRP sheets, *Ndt & E International* 43(7) (2010) 615-628.

526 [15] W.C. Choi, H.D. Yun, Acoustic emission activity of CFRP-strengthened reinforced concrete beams
527 after freeze–thaw cycling, *Cold Regions Science & Technology* 110 (2014) 47-58.

528 [16] A. Nair, C.S. Cai, F. Pan, X. Kong, Acoustic emission monitoring of damage progression in CFRP
529 retrofitted RC beams, 1(1) (2014) 111-130.

530 [17] E. Selman, A. Ghiami, N. Alver, Study of fracture evolution in FRP-strengthened reinforced concrete
531 beam under cyclic load by acoustic emission technique: An integrated mechanical-acoustic energy
532 approach, *Construction & Building Materials* 95 (2015) 832-841.

533 [18] P.R. Prem, A.R. Murthy, Acoustic emission and flexural behaviour of RC beams strengthened with
534 UHPC overlay, *Construction & Building Materials* 123(1) (2016) 481-492.

535 [19] S. Rouchier, G. Foray, N. Godin, M. Woloszyn, J.J. Roux, Damage monitoring in fibre reinforced
536 mortar by combined digital image correlation and acoustic emission, *Construction & Building Materials*
537 38(38) (2013) 371–380.

538 [20] M.K. Elbatanouny, P.H. Ziehl, A. Larosche, J. Mangual, F. Matta, A. Nanni, Acoustic emission
539 monitoring for assessment of prestressed concrete beams, *Construction & Building Materials* 58(58)
540 (2014) 46-53.

541 [21] M. Ohtsu, K. Mori, Y. Kawasaki, Corrosion Process and Mechanisms of Corrosion-Induced Cracks in
542 Reinforced Concrete identified by AE Analysis, *Strain* 47(s2) (2011) 179–186.

543 [22] J.H. Kurz, New approaches for automatic threedimensional source localization of acoustic
544 emissions--Applications to concrete specimens, *Ultrasonics* 63 (2015) 155-162.

545 [23] V. Janapati, F. Kopsaftopoulos, F. Li, J.L. Sang, F.K. Chang, Damage Detection Sensitivity
546 Characterization of Acousto-Ultrasound-based SHM Techniques, *Structural Health Monitoring* 15(2)
547 (2016) 143-161.

548 [24] R.V. Sagar, B.K.R. Prasad, R.K. Singh, Kaiser effect observation in reinforced concrete structures and
549 its use for damage assessment, *Archives of Civil & Mechanical Engineering* 15(2) (2014) 548-557.

550 [25] X. Fu, Q. Xie, L. Liang, Comparison of the Kaiser effect in marble under tensile stresses between the
551 Brazilian and bending tests, *Bull. Eng. Geol. Environ.* 74(2) (2015) 535-543.

552 [26] A. Lehtonen, J.W. Cosgrove, J.A. Hudson, E. Johansson, An examination of in situ rock stress
553 estimation using the Kaiser effect, *Eng. Geol.* 124 (2012) 24-37.

- 554 [27] E. Tuncay, Y. Obara, Comparison of stresses obtained from Acoustic Emission and Compact
555 Conical-Ended Borehole Overcoring techniques and an evaluation of the Kaiser Effect level, Bull. Eng.
556 Geol. Environ. 71(2) (2012) 367-377.
- 557 [28] K. Komloš, S. Popovics, T. Nürnbergerová, B. Babál, J.S. Popovics, Ultrasonic pulse velocity test of
558 concrete properties as specified in various standards, Cement & Concrete Composites 18(5) (1996)
559 357-364.
- 560 [29] C. Grosse, H. Reinhardt, T. Dahm, Localization and classification of fracture types in concrete with
561 quantitative acoustic emission measurement techniques, Ndt & E International 30(4) (1997) 223-230.
- 562 [30] D.G. Aggelis, T. Shiotani, Repair evaluation of concrete cracks using surface and
563 through-transmission wave measurements, Cement & Concrete Composites 29(9) (2007) 700-711.
- 564 [31] S. Momoki, T. Shiotani, H.K. Chai, D.G. Aggelis, Y. Kobayashi, Large-scale evaluation of concrete
565 repair by three-dimensional elastic-wave-based visualization technique, Structural Health Monitoring
566 12(3) (2013) 240-251.
- 567 [32] G. Karaiskos, E. Tsangouri, D.G. Aggelis, K. Van Tittelboom, N. De Belie, D. Van Hemelrijck,
568 Performance monitoring of large-scale autonomously healed concrete beams under four-point bending
569 through multiple non-destructive testing methods, Smart Materials & Structures 25(5) (2016) 055003.
- 570 [33] M. Ohtsu, Elastic wave methods for NDE in concrete based on generalized theory of acoustic
571 emission, Construction & Building Materials 122 (2016) 845-854.
- 572 [34] Partie, EUROCODE 2: DESIGN OF CONCRETE STRUCTURES. PART 1-1. GENERAL RULES AND RULES
573 FOR BUILDINGS 2004.
- 574 [35] G. Swit, Diagnostics of Prestressed Concrete Structures by Means of Acoustic Emission, The
575 Proceedings of 2009 International Conference on Reliability, maintainability and Safety, 2009, pp.
576 958-962.
- 577 [36] M.G.R. Sause, Investigation of Pencil-Lead Breaks as Acoustic Emission Sources, Journal of Acoustic
578 Emission 29(1) (2011) 184-196.
- 579 [37] A.H. Mattock, L.B. Kriz, E. Hognestad, Rectangular concrete stress distribution in ultimate strength
580 design.
- 581 [38] S.Y. Debaiky, E.I. Elniema, BEHAVIOR AND STRENGTH OF REINFORCED CONCRETE HAUNCHED BEAMS
582 IN SHEAR, Journal of the American Concrete Institute (1982).
- 583 [39] A.A. Committee, The shear strength of reinforced concrete members—slabs, Journal of the
584 Structural Division 99 (1973) 1091-1187.
- 585 [40] S. Liu, L. Zhang, Z. Chen, J. Zhou, C. Zhu, Mode-specific damage identification method for reinforced
586 concrete beams: Concept, theory and experiments, Construction & Building Materials 124 (2016)
587 1090-1099.
- 588 [41] E. Hognestad, N.W. Hanson, Mchenry, Douglas, Concrete Stress Distribution in Ultimate Strength

589 Design, Journal of the American Concrete Institute (1955).
590